Efficient FEM-DBEM coupled approach for crack propagation simulations

V. Giannella, M. Perrella, R. Citarella
Dept. of Industrial Engineering, University of Salerno, via G. Paolo II, 132, Fisciano (SA), Italy
e-mail: rcitarella@unisa.it

Abstract. The paper deals with a FEM-DBEM hybrid methodology applied to crack propagation simulations. The method allows to simulate cracks propagation by means of Finite Element Method (FEM) and Dual Boundary Element Method (DBEM), coupled in a procedure that optimise computational effort and accuracy. FEM is used for stress evaluation of the uncracked domain, whereas, the fracture analysis on a submodel embedding the cracked zone is demanded to DBEM. In particular, a DBEM submodel is extracted from the FEM model, a crack is introduced and traction boundary conditions are transferred from global FEM analysis to the crack surfaces of DBEM submodel (this will result the only needed boundary conditions to work out the DBEM analysis). The aforementioned tractions are those corresponding to the stresses calculated by a FEM global analysis along the virtual path traced by the DBEM advancing crack; consequently, a continuous exchange of data between FEM and DBEM environments is needed during the step by step crack propagation simulation.
The proposed case study is based on a shaft/hub coupling undergoing three different loading conditions: combined "bending" and "press-fit", "shear" and "torque". The material is a common steel with isotropic mechanical properties, whose Paris' parameters are calibrated at room temperature. *J*-integral and Minimum Strain Energy Density (MSED) methods are chosen for Stress Intensity Factors (SIFs) and crack path assessment respectively.
A sound agreement is shown among SIFs calculated with the proposed Loaded Crack (LC) method and those evaluated by a "classical" FEM-DBEM approach, where displacement or traction boundary conditions, again retrieved from a FEM analysis of the uncracked global model, are applied on all DBEM submodel cut surfaces.

Keywords: FEM, DBEM, superposition principle, crack propagation

1. Introduction

In order to ensure the operation of a mechanical component with the constraint of a required fatigue life, it is necessary to carry out a fracture mechanics assessment under the general framework of *damage tolerance*. The fatigue growth analysis of surface cracks is one of the most important parts for structural integrity prediction of the cylindrical metallic components (bars, wires, bolts, shafts, etc.) in the presence of initial and accumulated in-service damages. Part-through flaws appear on the free surface of cylindrical components and, frequently, their shape assumes a typical semielliptical geometry. Multiaxial loading conditions, including tension/compression, bending and torsion, are usual for cylindrical metallic components of engineering structures. Therefore, the problem of residual fatigue life prediction of such type of structural elements is complex and a closed-form solution is often not available because surface flaws are three-dimensional in nature and load combinations can lead to mixed-mode conditions.
Among the methodologies used to simulate the fracture behaviour of complex structures, the Finite Element Method (FEM) is largely adopted. However, modelling crack growth with FEM makes the remeshing process during crack propagation particularly demanding, especially under mixed-mode loading conditions [1-3]. Hence, standing the difficulty to apply and to keep under control any automated remeshing algorithm, eXtended Finite Element Method (XFEM) and meshless methods have been widely applied to crack propagation simulations in the last years. Alternatively, special purpose elements can be implemented for the FEM simulations, in order to embed a micromechanical damage model in the material law [4]. These techniques allow for a mesh independent crack

representation since remeshing is not required for crack growth modelling [5-6]. The drawback of such mesh independency consists of a high complexity of element formulation, material law and solver algorithm.
The Dual Boundary Element Method (DBEM) simplifies the meshing process and accurately characterizes the singular stress fields near the crack front [2, 7], but, what is more important, can efficiently work together with FEM in a coupled approach [8-11], particularly when tackling simulations of large structures [12-15]. As a matter of fact, a coupled FEM-DBEM approach is here adopted since it combines the advantages of FEM in dealing with complex analyses with the benefits of DBEM when tackling fracture problems.
Generally, a FEM approach is used to solve the global problem and assess displacement/stress/strain fields, useful to extract the boundary conditions to be applied on a DBEM submodel extracted from such FEM model.
In a "classical" approach the DBEM submodel crack-growth simulation is performed under displacements or traction boundary conditions on the cut surfaces, without updating of their values during the propagation; such boundary conditions are consequently hypothesized to be insensitive to the submodel stiffness variation due to the crack growth. In the former case, the approach provides non-conservative results in terms of residual life cycles whereas, in the latter case, conservative results are obtained. Interestingly the proposed approach provides crack growth results in between the two.
The current paper presents such alternative FEM-DBEM submodelling approach applied to fracture problems: it is based on the principle of linear superposition and applicable when just the calculation of Stress Intensity Factors (SIFs) is needed, namely, the stress-strain assessment throughout the whole submodel is not required; the only boundary conditions transferred from FEM solution to DBEM submodel are represented by a load distribution to apply on the crack faces.
The theoretical background is well detailed in [16], where Wilson et al. reformulated *J* integral approach for thermal-stress problems and showed how to calculate Stress Intensity Factors (SIFs) by a simple application of a load distribution on crack faces. In particular, it was shown the possibility to formulate a thermal-stress crack problem in terms of a crack surface loading problem by using the principle of linear superposition, namely the crack growth simulations are performed by using a DBEM submodel, containing a crack, loaded with tractions calculated a priori solving an uncracked global FEM model.
As a matter of fact, in this work, SIFs are calculated using the *J*-integral formulation [17, 18]; then, the range of SIFs ΔK (or ΔK_{eff} in a mixed mode problem) is used as the crack driving force to obtain the corresponding crack growth rate *da/dN* whereas the crack path is evaluated by means of the Minimum Strain Energy Density (MSED) criterion [19].
Notably, the uncracked FEM model containing the different loading conditions is necessary just to compute accurately the stress field in the surroundings of what will be the considered cracked zone, whereas, the fracture problem solution is completely demanded to the DBEM environment. All the loads applied to the real component (e.g. thermal, electro-magnetic, gravity, etc.) are solely considered during the global FEM analysis; then this approach provides the SIFs evaluation and subsequently the whole crack-growth evolution by means of step-by-step pure stress analyses on the DBEM submodel.
A further advantage of such approach is given by the possibility to study a crack propagation with a significantly smaller model than that typically needed in a "classical" FEM-DBEM implementation. As a matter of fact, the applied load is self-equilibrated, with rapidly vanishing stresses when getting far apart from the crack: the minimal submodel size is dictated by the need to guarantee a complete stress relief in correspondence of boundaries. Resizing the DBEM submodel permits to speed up the calculations as a consequence of a smaller system of equations to solve.
The adopted FEM and DBEM commercial codes are respectively ABAQUS [20] and BEASY [21].
Results provided by the newly proposed procedure are then compared with those obtained by pure DBEM analyses, extended to the whole model (no submodelling).

2. Case study

The selected case study, proposed by dr. G. Dhondt (MTU Aeroengines) in an attempt to enhance the level of mode mixity against a similar configuration analysed in [22], represents a hub and a hollow shaft, in a geometric configuration symmetric with respect to a mid-plane perpendicular to the shaft

axis (Fig. 1). The material is a steel, whose behaviour is assumed as linear-elastic, with Young's modulus E = 210 GPa and Poisson's ratio ν= 0.3.
The crack geometry is a planar semi-elliptical part-through crack, initiated from the external surface of the shaft, having dimensions of a = 1.9 mm and c = 3.8 mm (Fig. 1a).

Fig. 1a: Drawings of the shaft with highlight of the crack and fillet radii.

Fig. 1b: Drawings of the hub; the dotted red line shows the loading application zone.

Three different loading conditions have been applied to the model as shown in Fig. 2:

- "coupled" (Fig. 2a): consisting of a uniform traction distribution on the shaft end surface, with resultant magnitude equal to 200 kN, and a corresponding point force on the hub with same magnitude and opposite direction; such load case is coupled with a press fit condition of 0.28 mm at shaft/hub contact surface where a static friction coefficient μ=0.6 is considered;
- "shear" (Fig. 2b): consisting of a uniform traction distribution, with resultant magnitude equal to 200 kN, along the hub perimeter line (dotted red line of Fig. 1b);
- "torque" (Fig. 2c): consisting of a uniform torque distribution, with resultant magnitude equal to 22.5 kNm, again distributed along the hub perimeter line (dotted red line of Fig. 1b.

(a) (b) (c)
Fig. 2: Considered load cases: "coupled" (a), "shear" (b) and "torque" (c).

3. Loaded Crack (LC) approach

The proposed approach is based on the application of the superposition principle to fracture mechanics problems. Such an approach can be described assuming the more general thermal-stress crack problem (our case is a pure stress problem) schematically shown in Fig. 3 [see also 16]:

- starting from an original uncracked domain (*a*), a crack can be opened (*b*) and loaded with tractions equal to those calculated over the dashed line of the virtual crack in (*a*);
- the new configuration (*b*), perfectly equivalent to the previous one (*a*), can be transformed by using the superposition principle, splitting the boundary conditions as provided in (*c*) and (*d*) (Eq. 1): (*c*) represents the original problem to solve, whereas (d), after the tractions sign inversion turn in the equivalent problem (e) that will be effectively worked out; namely, SIFs for case (c) are equal (Eq. 2) to those calculated for the simpler problem (e).

In conclusion, using boundary conditions retrieved from the considered thermal-stress uncracked problem (a) a purely stress crack problem (*e*) can be solved, in which, the crack faces undergo tractions equal in magnitude but opposite in sign to those calculated over the dashed line in (*a*).

Fig. 3. Superposition principle applied to fracture thermo-mechanical problems ("T" indicates a temperature distribution throughout the domain).

$$K_a = K_b = 0 = K_c + K_d \tag{1}$$

$$K_c = -\ K_d = K_e \tag{2}$$

4. J-integral formulation

In three-dimensional problems, *J*-integral can be defined as:

$$J = \int_{\Gamma_\rho} \left(W n_1 - \sigma_{ij} \frac{\partial u_i}{\partial x_1} n_j \right) d\Gamma = \int_C \left(W n_1 - \sigma_{ij} \frac{\partial u_i}{\partial x_1} n_j \right) d\Gamma +$$

$$+\int_{\omega}\left(Wn_1-\sigma_{ij}\frac{\partial u_i}{\partial x_1}n_j\right)d\Gamma+\int_{C_\rho}\frac{\partial}{\partial x_3}\left(\sigma_{i3}\frac{\partial u_i}{\partial x_1}\right)d\Omega \quad (3)$$

Fig. 4. Closed path around the crack tip.

Where Γ_ρ is the total closed path enclosing the crack tip, *J*-integral is defined in the plane with equation $x_3 = 0$ for a generic position on the crack front (Fig. 4). In the general case of free crack faces ($\sigma_{ij} = 0$ along path ω), the contributions to the *J*-integral for both crack faces vanish whereas, in case of loaded crack faces, the contribution along path *C* vanishes.
In mixed mode problems, the J-integral is related to the three basic fracture modes by the components J^I, J^{II} e J^{III}:

$$J = J^I + J^{II} + J^{III}$$

Rigby and Aliabadi [17-18] presented a decomposition method through which integral J^I, J^{II} e J^{III} in elastic problems can be calculated directly from *J*. Firstly, *J* was divided into two components:

$$J = J^S + J^{AS}$$

J^S and J^{AS} are obtained, respectively, from symmetric and anti-symmetric elastic field around the crack plane. When the elastic field of mode I (opening mode) is symmetric in the crack plane, then it happens that

$$J^S = J^I \qquad \text{and} \qquad J^{AS} = J^{II} + J^{III}$$

J^{II} and J^{III} integrals can be calculated from J^{AS} making an additional analysis on the anti-symmetric field. Then, when *J*-integral is calculated as sum of the three separated contributions of mode I, II and III, Stress Intensity Factors can be obtained (Eq. 4) [18]:

$$J_1 = J^I + J^{II} + J^{III} = \frac{1}{E'}\left(K_I^2 + K_{II}^2\right) + \frac{1}{2\mu}K_{III}^2 \quad (4)$$

where μ is the rigidity modulus and $E' = E$ (Young's modulus) for plane stress, or $E' = \frac{E}{1-\nu^2}$ for plane strain state.

5. FEM and DBEM models

5.1 Coupled approach

The global FEM model (Fig. 5a) consists of a half part of hub/shaft coupling. The related load boundary conditions are presented in Fig. 2. The FE mesh is based on nearly 84000 quadratic hexahedral elements.
Then, a FEM submodel (Fig. 5b), containing a small portion of the shaft, is extracted from the global model. Such submodel, containing only the volume surrounding the crack insertion point, has size and mesh refinement capable to guarantee a higher (than that provided by the global model) accuracy when evaluating the stress field in the neighbourhood of the crack. In particular, the stresses along the virtual surface traced by the crack have to be evaluated with the highest possible precision, because they represent the (only) driving force for the following DBEM crack propagation. To get the needed precision, especially for the "torque" load case, it has been necessary to strongly refine the FEM submodel mesh. This is due to the high kink angles for the torque load case (nearly 90° for the initial propagation steps) that requires heavy DBEM mesh refinements and smaller crack advances per step.
Subsequently, a BEM submodel (Fig. 5c) is created containing the zone surrounding the crack initiation point (the crack is not yet modelled and that is why the DBEM formulation is not yet

enforced). In addition to the FEM stresses, applied as tractions to the crack faces (Fig. 5d), springs of negligible stiffness (in purple in Fig. 5c) are applied to a few BEM elements in order to prevent rigid body motion. Due to the loading conditions consisting of a self-equilibrated load, a large part of the DBEM cracked submodel (now the crack has been introduced with automatic remeshing in the surrounding area) turns out to have a null stress field. For this reason, the fracture problem can be analysed considering a very small portion of the global FEM model, with inherent decrease of the needed computational effort.
The FEM submodel (Fig. 5b), when used for the "coupled" and "shear" load cases, is made up of nearly 25000 quadratic hexahedral elements whereas, for the "torque" load case is made up of nearly 130000 quadratic hexahedral elements (Fig. 6c).

(a) (b) (c) (d)

Fig. 5. FEM global model (a), FEM submodel (b), BEM model (c), DBEM model (d) close-up of the inserted crack and highlight of tractions applied to the crack faces.

A preliminary study was aimed at assessing the minimum needed dimensions of the BEM submodel, useful to guarantee a complete extinction of stresses from the crack area to the boundaries. Such uncracked BEM model comprises nearly 1200 linear elements and this number rises up to nearly 1800 when the initial crack is inserted. The remeshing zone and the crack faces are discretised with 9-noded quadratic elements whereas 4-noded linear elements are used for the bulk of the remaining mesh.

5.2 Pure DBEM model

The DBEM global model is made up of two different zones (one for the shaft and the other for the hub), with a mesh of quadrilateral boundary elements with quadratic shape functions.
Consistently with the description given in section 2, the "coupled" load case (Fig. 2a) is obtained by superimposing a uniform traction distribution on the shaft end surface and a point force on the hub to a press-fit condition at shaft-hub interface. The "shear" load case (Fig. 2b) is obtained by applying a uniform traction distribution along the depicted red line. In the "coupled" and "shear" load case, the shaft symmetry plane is fully clamped. Finally, the "torque" load case (Fig. 2c) consists of tangential tractions uniformly distributed along the same line as in the "shear" load case; here, the clamping on the symmetry plane surface is removed and replaced with an antisymmetry boundary condition.

(a) (b) (c)

Fig. 6. (a) DBEM un-cracked model; (b) close-up of the remeshed area surrounding the crack insertion point; (c) details of the initial crack geometry with J-paths along the crack front (purple) for the J-integral computation.

A part-through semi-elliptical crack was inserted on the shaft external surface (Fig. 6b). After crack insertion (Fig. 6c), fully automatic together with the inherent local remeshing with triangular boundary elements, the number of elements increased from 2500 to nearly 3100.

6. FEM results

The FEM global model is loaded considering the aforementioned load cases (Fig. 2), whose related stress fields are computed and shown in Fig. 7. Subsequently, using a finer mesh, a FEM submodel is extracted to compute with higher accuracy the stress-strain field in the crack neighbourhood (Fig. 7).

(a)
(b)
(c)
Fig. 7. FEM von Mises stresses calculated for “coupled” (a) and “shear” (b) load cases. For “torque” load case, shear stress τ_{XZ} are displayed (c).

7. DBEM and FEM-DBEM LC results

7.1. Comparison of SIFs for the initial crack configuration, by pure DBEM and FEM-DBEM LC approaches

FEM results are used to determine the boundary conditions for the crack propagation simulation in the DBEM submodel. The stress-strain results from DBEM submodel analyses (Fig. 8) are completely different in comparison to the corresponding results obtained by the FEM analyses, but this was expected in light of application of superposition principle as previously detailed. The DBEM solution is just aimed at properly characterizing the crack tip stress behaviour in order to correctly compute SIFs, but cannot provide a realistic stress scenario throughout the domain.

(a)
(b)
(c)
Fig. 8. Von Mises stresses for the DBEM models undergoing the load cases: “coupled” (a), “shear” (b) and “torque” (c).

The DBEM results are computed modelling the crack directly in a DBEM shaft/hub assembly (Fig. 6), loaded with remote loading conditions, as in the current global FEM analyses.
SIFs calculated with the proposed coupled FEM-DBEM LC approach are compared to those obtained with a pure DBEM analysis (Fig. 9) showing a good agreement.
A synthetic quantitative assessment of discrepancies can be provided considering the effective SIF computed by the Yaoming-Mi formula (Eq. 5) [23]: the percentage differences between DBEM and FEM/DBEM LC are lower than 1.1%, 2.2% and 0.1% for “coupled”, “shear” and “torque” load cases respectively.

$$K_{eff} = \sqrt{\left(K_I + |K_{III}|\right)^2 + 2K_{II}^2} \tag{5}$$

(a)
(b)
(c)
Fig. 9. SIFs comparison between FEM-DBEM LC and pure DBEM methods: “coupled” (a), “shear” (b) and “torque” (c).

7.2. Comparison of crack propagations for the initial crack configuration, by pure DBEM and FEM-DBEM LC approaches

FEM-DBEM crack propagations are worked out with the proposed LC approach. When SIFs are computed and the new crack front is predicted, new surface resulting from crack extension has to be loaded by additional tractions, coming from the FEM stress field computed at the updated virtual crack spatial configuration. Then a new DBEM analysis is performed and the propagation proceeds step-by-step.
The Paris’ law coefficients are C=1.23085E-12 [MPa*mm$^{0.5}$] and the n =2.8.
The DBEM crack propagation simulation is divided into four separate phases:

- “crack adder” - the crack is inserted into the DBEM model and loaded by a FEM-DBEM interface routine;
- “solver” - the cracked DBEM model is solved and the stress field and corresponding SIFs are calculated;
- “crack life predictor” - the adopted crack growth law is used to predict the fatigue cycles corresponding to the i_{th} crack advance;
- “crack extender” - the crack is extended and the next configuration is used to continue the analysis.

The average crack advance per step and the number of steps were chosen for each load condition as:

- “coupled” - 20 steps with average crack extension distance per step equal to 0.5 mm;
- “shear” - 20 and 10 steps with average crack extension distance per step equal to 0.5 mm and 1 mm, respectively;
- “torque” - 30 steps with average crack extension distance per step ranging between 0.08 and 0.25 mm.

Crack size vs. life cycles curves are plotted in Fig. 10 for the three different loading conditions. Such results are compared with those obtained by a pure DBEM approach, directly applied to the global assembly solution, displaying a good agreement.
Crack size c is the distance between the crack insertion point and the crack front midpoint; crack size a and b are the distances between the crack insertion point and the break through points, measured along the intersection lines between the crack edges and the shaft external surface (see Fig. 11).

Both crack wings, during propagation, proceeds symmetrically in “coupled” and “shear” load cases, whereas, for the “torque” load case a difference between the two growing wings emerges, attributable to the different impact of the shaft fillet radii on the two crack tips.
Stress fields for the final cracked configuration of the three load cases are shown in Fig. 12: von Mises stresses for “coupled” (Fig. 12a) and “shear” (Fig. 12b), shear stress τ_{XZ} for “torque” (Fig. 12c).
The final crack shapes are shown in Fig. 13, in which the normal tractions, provided by the FEM global analysis, are plotted as applied to the crack surface; moreover, the *J*-paths (internal contours in which *J* integral are calculated) at discrete positions along the crack fronts are visible.

(a) (b) (c)
Fig. 10. Crack size vs cycles. Comparison between FEM-DBEM LC and DBEM methods: “coupled” (a), “shear” (b) and “torque” (c).

Fig. 11. Crack size definitions.

(a) (b) (c)
Fig. 12. Von Mises stress fields at the end of the propagations: “coupled” (a), “shear” (b) and “torque” (c)
(c)
(a)
(b)
(c)
Fig. 13. Contour plots of normal tractions (MPa) as applied to final crack: “coupled” (a), “shear” (b) and “torque” (c).

7.3. Runtimes comparison

Runtimes for performing the various crack propagation simulations are now compared between FEM-DBEM LC and DBEM approaches. Average runtimes calculated for one step during simulations are listed in Tab. 1 (runtimes for the solution at each crack growth step change along the propagation due to the increasing number of elements needed to discretise the crack and adjacent surfaces, so that an average value was calculated). Runtimes are comprehensive of the four abovementioned intermediate phases (§7.2) of DBEM analysis, but just the crack insertion and solving phases play a significant role. The LC approach, in addition, needs the crack loading phase after crack insertion (the related runtimes are considered in the crack introduction phase).

Table 1 shows that FEM-DBEM LC approach takes nearly half of the time required for the same calculation using DBEM. This was expected since the LC model is smaller than the pure DBEM one. Furthermore, when considering more complex FEM models (e.g. with allowance for non-linear contacts, thermal loads, etc.), such gap becomes more pronounced, since such complexity does not affect the DBEM LC calculation where simple pure stress analyses are needed.

On the other hand, the crack loading phase can be very time consuming when using large FEM meshes that the DBEM code must handle per each growth step in order to properly transfer the needed data. This is highlighted by the "torque" load case analysis, in which the sharp crack kinking during the initial propagation steps imposes very small crack extensions distances and, consequently, a finer FEM mesh (see Fig. 7c). This problem can be overcome by using a smaller FE submodel and/or by optimizing the FEM mesh on the existing submodel.

Tab. 1. Average runtime during simulation.

Load case	*FEM-DBEM LC crack introduction*	*FEM-DBEM LC solution*	*DBEM crack introduction*	*DBEM solution*
Coupled	7 min.	14 min.	5 min.	41 min.
Shear	7 min.	17 min.	5 min.	47 min.
Torque	126 min.	162 min.	27 min.	303 min.

8. Conclusions

An efficient FEM-DBEM coupled procedure has been proposed for crack propagation simulations. Such a procedure, based on the principle of linear superposition, enables to compute SIFs with high accuracy resorting to just a simple kind of boundary condition for the DBEM analyses: a self-equilibrated load distribution applied on the crack faces.

A benchmark of this alternative Loaded Crack LC approach against a purely DBEM procedure has been arranged, showing a very good agreement between SIFs and crack growth rates.

The LC approach is fully automated and permits to predict SIFs with lower runtimes than pure DBEM approach thanks to smaller DBEM models. Such an approach is also more accurate than the FEM-DBEM coupled procedure based on the application of boundary conditions on the submodel cut surfaces. In the latter case, the boundary conditions are obtained by an uncracked FEM model and, typically, are not updated along the crack growth, introducing some approximation. On the contrary, the LC approach updates continuously (step-by-step) the tractions applied on the crack faces adding new loads in correspondence to the newly added crack surfaces. Such tractions are obtained from an uncracked FEM configuration but, consistently with the superposition principle, this does not represent any additional approximation.

Furthermore, the LC approach allows an accurate SIFs assessment, working on DBEM pure stress analyses and demanding more complex global analyses (i.e. with allowance for nonlinearities) to the FEM step. This point represents a remarkable advantage of the proposed hybrid FEM-DBEM approach because the FEM versatility in solving complex problems is coupled with the DBEM accuracy when handling fracture problems.

References

[1] R. Citarella, M. Lepore, A. Maligno, V. Shlyannikov, FEM simulation of a crack propagation in a round bar under combined tension and torsion fatigue loading, Frattura ed Integrità Strutturale 31 (2015) 138-147.

[2] R. Citarella, G. Cricrì, Comparison of DBEM and FEM crack path predictions in a notched shaft under torsion, Eng. Fract. Mech. 77 (2010) 1730–49.

[3] R. Citarella, G. Cricrì, M. Lepore, M. Perrella, DBEM and FEM Analysis of an Extrusion Press Fatigue Failure, in: A. Öchsner, L.F.M. da Silva, H. Altenbach (Eds.), Materials with Complex Behaviour–Advanced Structured Materials, Springer-Verlag, Berlin, Germany, 2010, Vol. 3, Part 2, 181-191.

[4] G. Cricrì, A consistent use of the Gurson–Tvergaard–Needleman damage model for the R-curve calculation, Frattura ed Integritá Strutturale 24 (2013) 161–74.

[5] Z. Goangseup, S. Jeong-Hoon, E. Budyn, L. Sang-Ho, T. Belytschko, A method for growing multiple cracks without remeshing and its application to fatigue crack growth, Model. Simul. Mater. Sci. Eng. 12 (2004) 901–15.

[6] D.L. Chopp, N. Sukumar, Fatigue crack propagation of multiple coplanar cracks with the coupled extended finite element/fast marching method, Int. J. Eng. Sci. 41 (2003) 845–69.

[7] R. Citarella, F.-G. Buchholz, Comparison of DBEM and FEM Crack Path Predictions with Experimental Findings for a SEN-Specimen under Anti-Plane Shear Loading, Key Engineering Materials (2007), vol. 348-349, p. 129-132.

[8] R. Citarella, G. Cricrì, M. Lepore, M. Perrella, Assessment of crack growth from a cold worked hole by coupled FEM-DBEM approach, Key Engineering Materials 577-578 (2014), 669-672.

[9] R. Citarella, P. Carlone, R. Sepe, M. Lepore, DBEM crack propagation in friction stir welded aluminum joints, Advances in Engineering Software 101 (2016) 50–59.

[10] P. Carlone, R. Citarella, M. R. Sonne, J. H. Hattel, Multiple crack growth prediction in AA2024-T3 friction stir welded joints, including manufacturing effects, International Journal of Fatigue 90 (2016) 69–77.

[11] R. Citarella, P. Carlone, M. Lepore, R. Sepe, Hybrid technique to assess the fatigue performance of multiple cracked FSW joints, Engineering Fracture Mechanics 132 (2016) 38-50.

[12] R. Citarella, V. Giannella, E. Vivo, M. Mazzeo, FEM-DBEM approach for crack propagation in a low pressure aeroengine turbine vane segment, Theoretical and Applied Fracture Mechanics, Volume 86, Part B, 2016, Pages 143–152.

[13] R. Citarella, G. Cricrì, Three-Dimensional BEM and FEM Submodelling in a Cracked FML Full Scale Aeronautic Panel, Appl. Compos. Mater. 21 (3) (2014) 557-577.

[14] R. Citarella, M. Lepore, M. Perrella and J. Fellinger, Coupled FEM–DBEM approach on multiple crack growth in cryogenic magnet system of nuclear fusion experiment 'Wendelstein 7-X', Fatigue Fract. Engng. Mater. Struct. 39 (2016) 1488–1502.

[15] R. Citarella, G. Cricrì, M. Lepore, M. Perrella, Thermo-mechanical crack propagation in aircraft engine vane by coupled FEM-DBEM approach, Advances in Engineering Software 67 (2014) 57-69.

[16] W.K. Wilson, I-W. Yu, The use of the J-integral in thermal stress crack problems, Int. J. Fract. 15 (1979) 377-387.

[17] R.H. Rigby, M.H. Aliabadi, Mixed-mode J-integral method for analysis of 3D fracture problems using BEM, Engng. Anal. Boundary Elem. 11 (1993) 239–56.

[18] R.H. Rigby, M.H. Aliabadi, Decomposition of the mixed-mode J-integral – revisited, Int. J. Solids Struct. 35(17) (1998) 2073–99.

[19] G.C. Sih, Strain energy density factor applied to mixed mode crack problems, Int. J. Fract. 10 (1974) 305-321.

[20] Dassault Systems Simulia Corp., Abaqus Analysis User's Manual, Version 6.12.1, Providence, RI, USA, (2011).
[21] BEASY V10r16, Documentation. C.M. BEASY Ltd., (2011).
[22] R. Citarella, V. Giannella, M. Lepore, DBEM crack propagation for nonlinear fracture problems, Frattura e Integrità Strutturale, 34 (2015) 514-523.
[23] Y. Mi, Three Dimensional Dual Boundary Element Analysis of Crack Growth, Ph.D. Thesis, University of Portsmouth, USA, (1995).

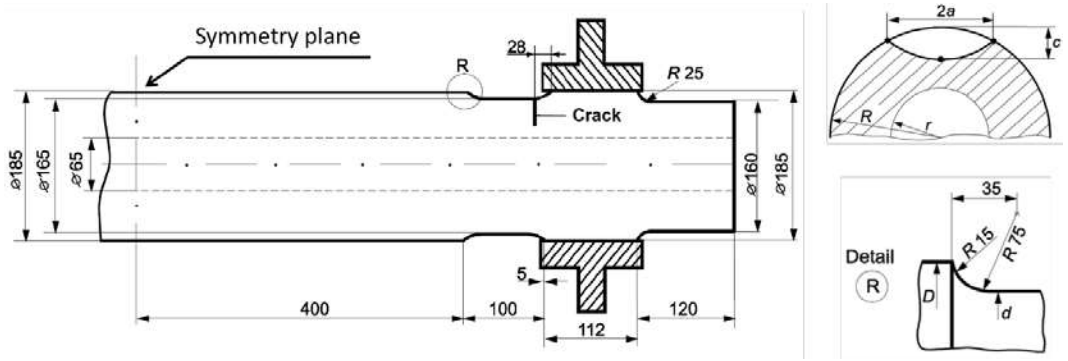

Fig. 1a: Drawings of the shaft with highlight of crack and fillet radii.

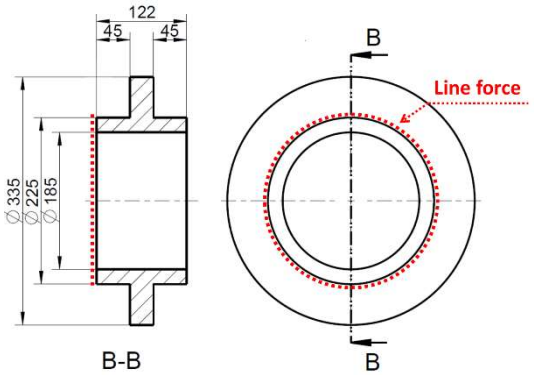

Fig. 1b: Drawings of the hub; the dotted red line shows the loading application zone.

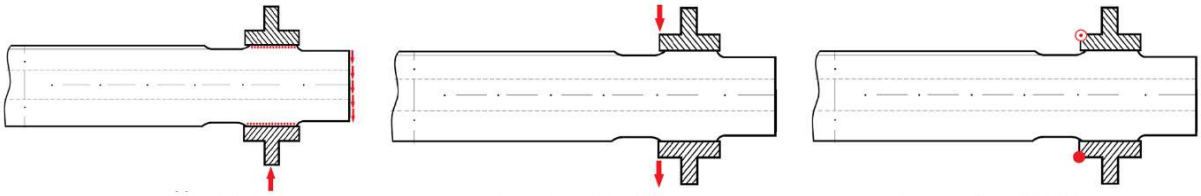

(a) (b) (c)

Fig. 2: Considered load cases: “coupled” (a), “shear” (b) and “torque” (c).

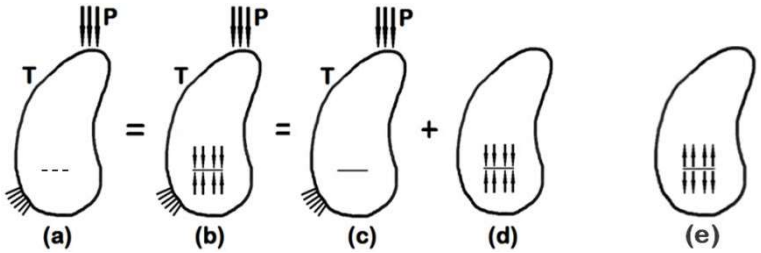

Fig. 3. Superposition principle applied to fracture thermo-mechanical problems (“T” indicates a temperature distribution throughout the domain).

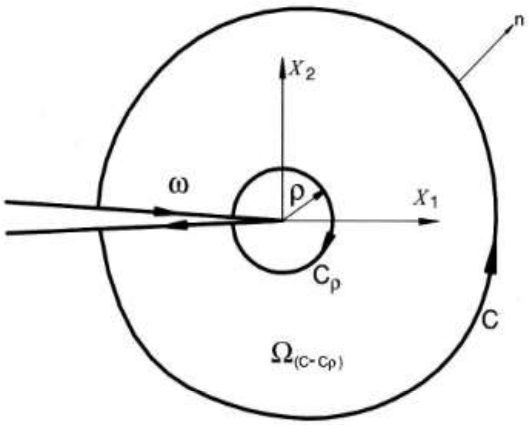

Fig. 4. Closed path around crack tip.

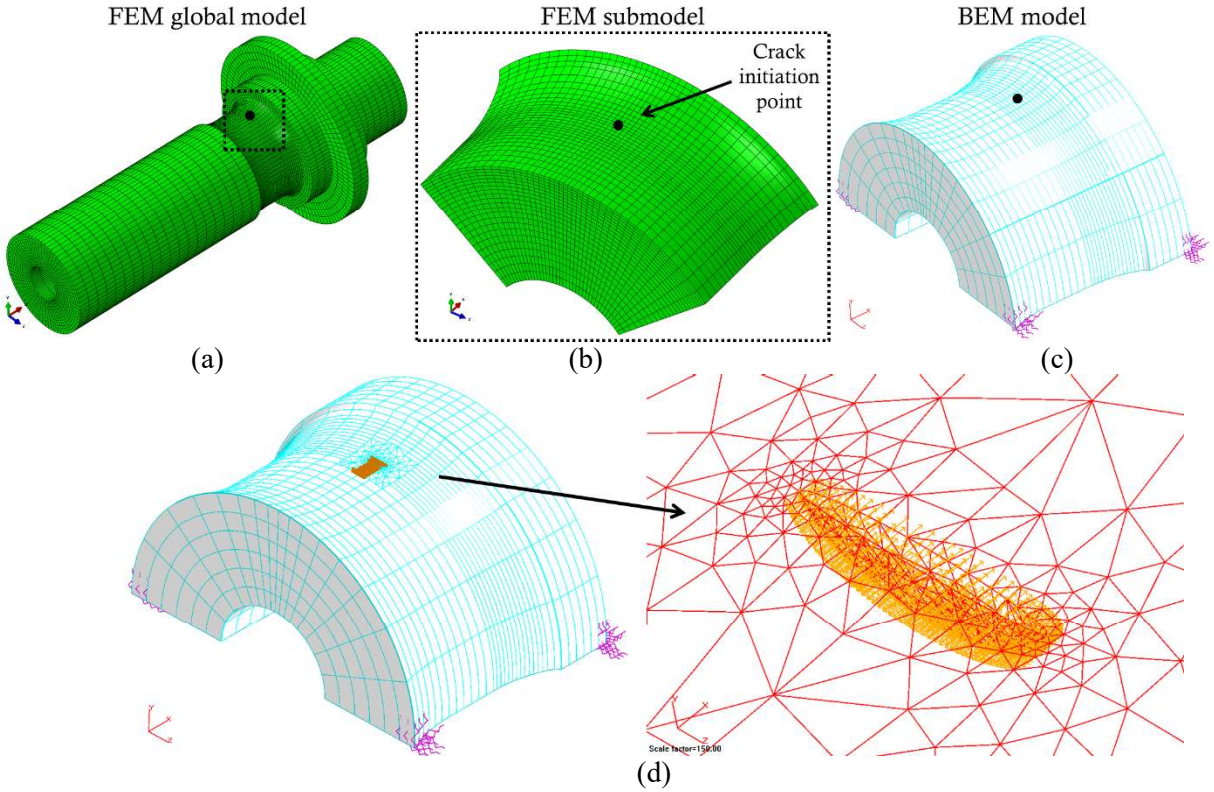

Fig. 5. FEM global model (a), FEM submodel (b), BEM model (c), DBEM model (d) with close-up of the inserted crack and highlight of tractions applied to crack faces.

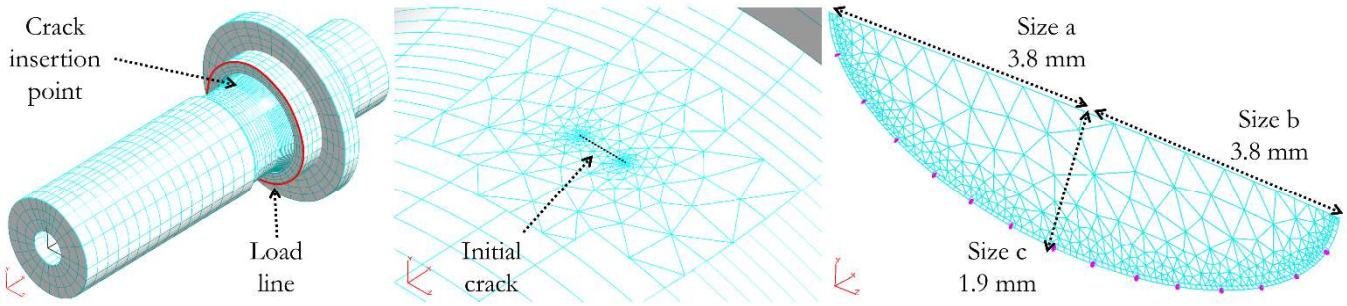

(a) (b) (c)

Figure 6: (a) DBEM un-cracked model; (b) close-up of the remeshed area surrounding the crack insertion point; (c) details of the initial crack geometry with J-paths along the crack front (purple) for the J-integral computation.

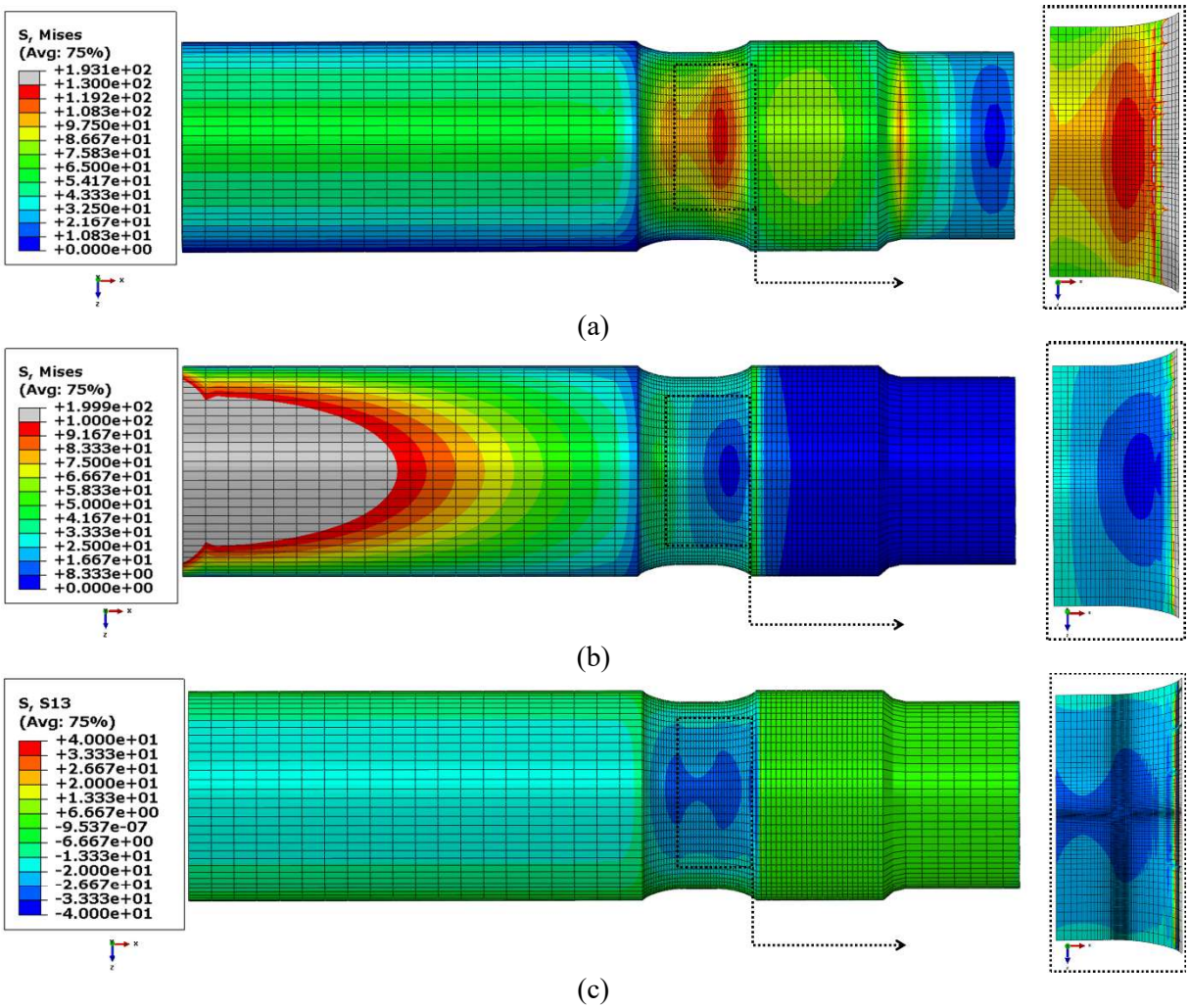

Fig. 7. FEM von Mises stresses calculated for "coupled" (a) and "shear" (b) load cases. For "torque" load case shear stress τ_{XZ} are displayed (c).

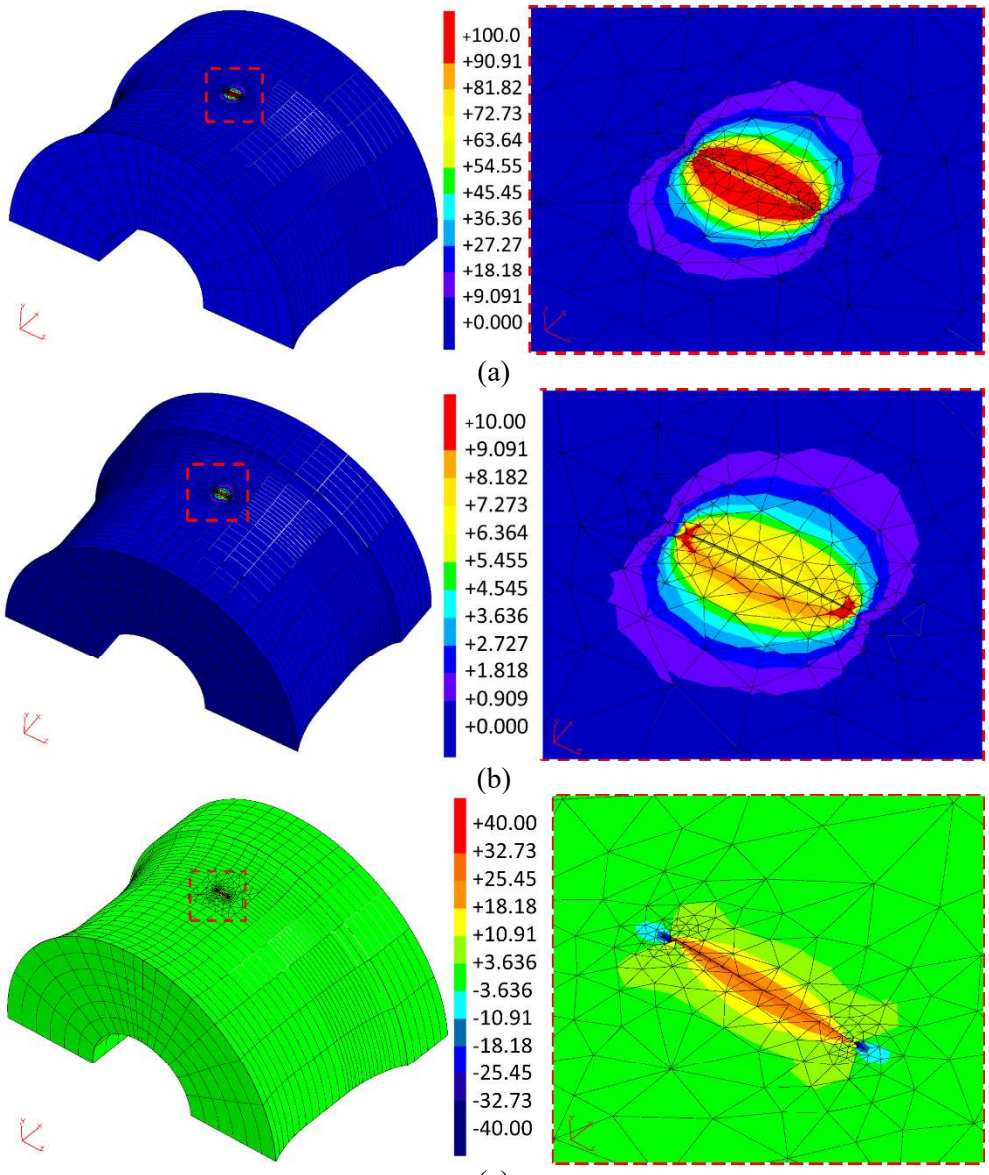

Fig. 8. Von Mises stresses for the DBEM models undergoing the load cases: “coupled” (a), “shear” (b), “torque” (c).

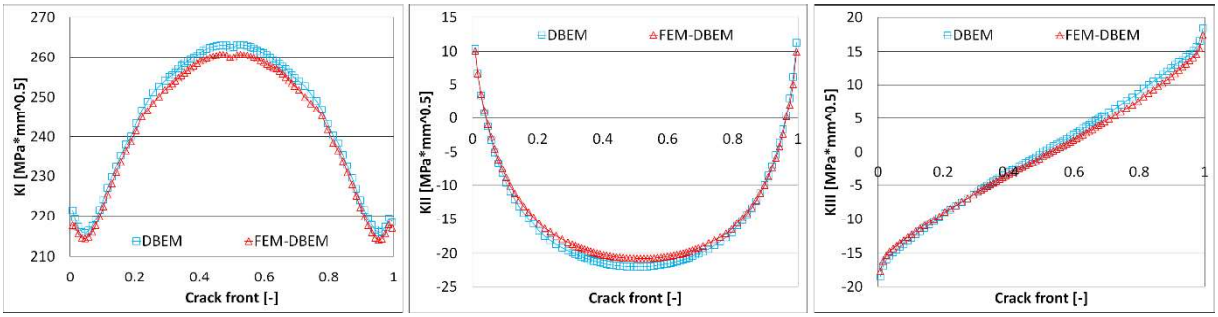

(a)

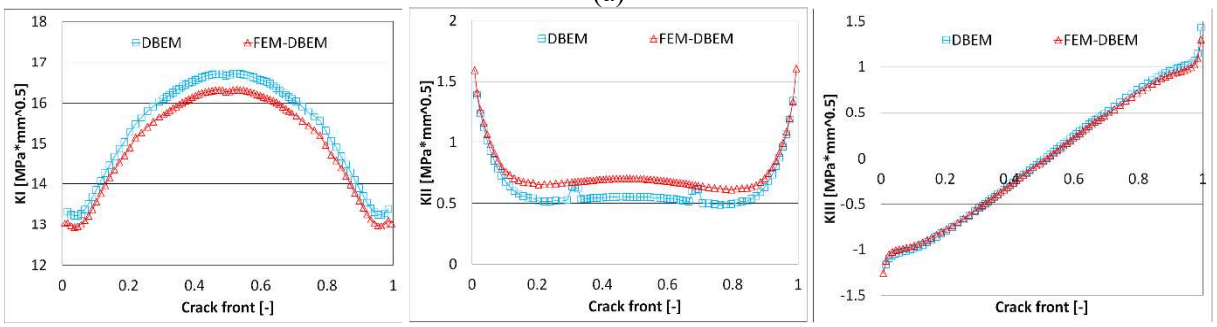

(b)

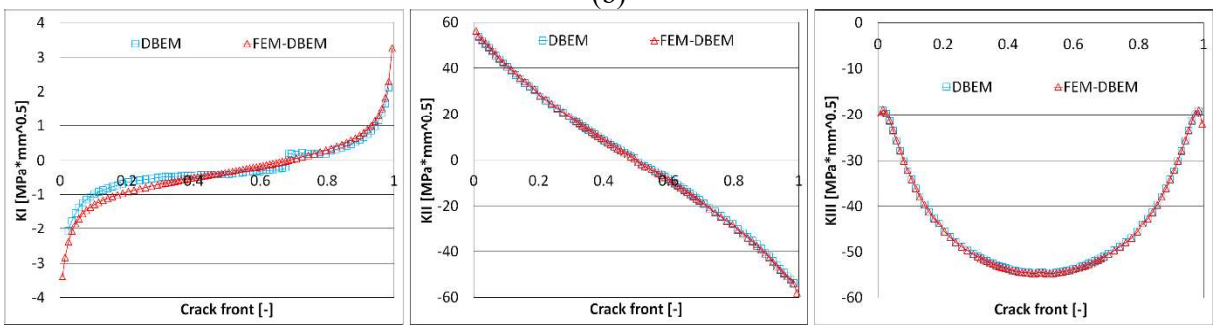

(c)

Fig. 9. SIFs comparison between FEM-DBEM LC and pure DBEM methods: “coupled” (a), “shear” (b), “torque” (c).

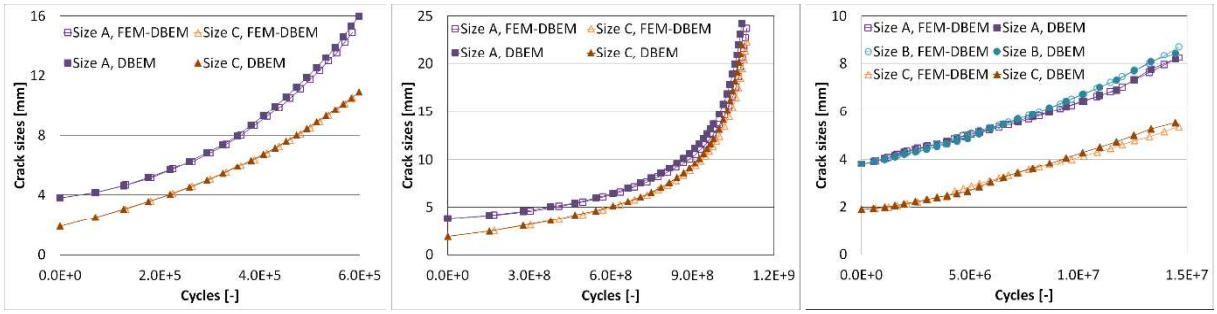

(a) (b) (c)

Fig. 10. Crack sizes vs Cycles comparison between FEM-DBEM LC and DBEM methods: “coupled” (a), “shear” (b), “torque” (c).

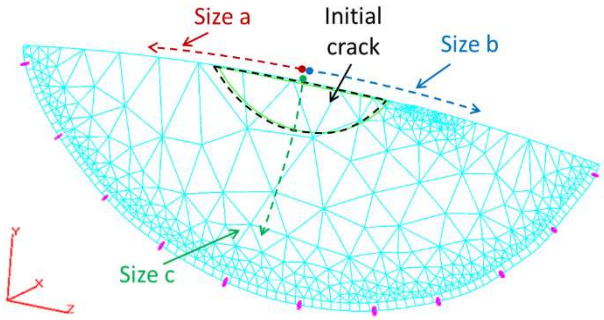

Figure 11: Crack size definitions.

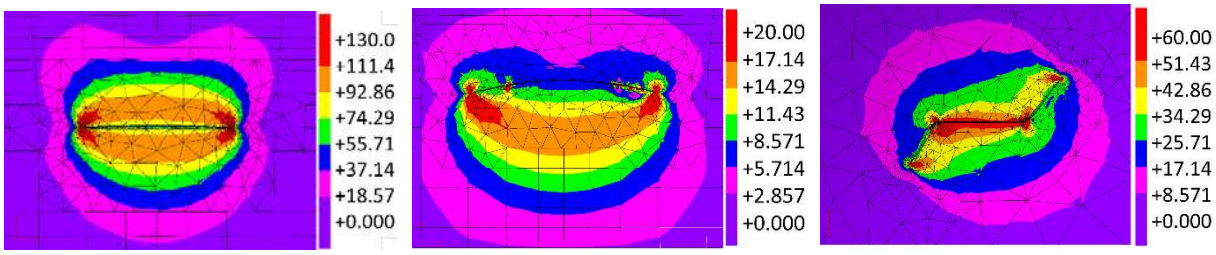

(a) (b) (c)

Fig. 12. Von Mises stress fields at the end of the propagations: “coupled” (a), “shear” (b), “torque” (c).

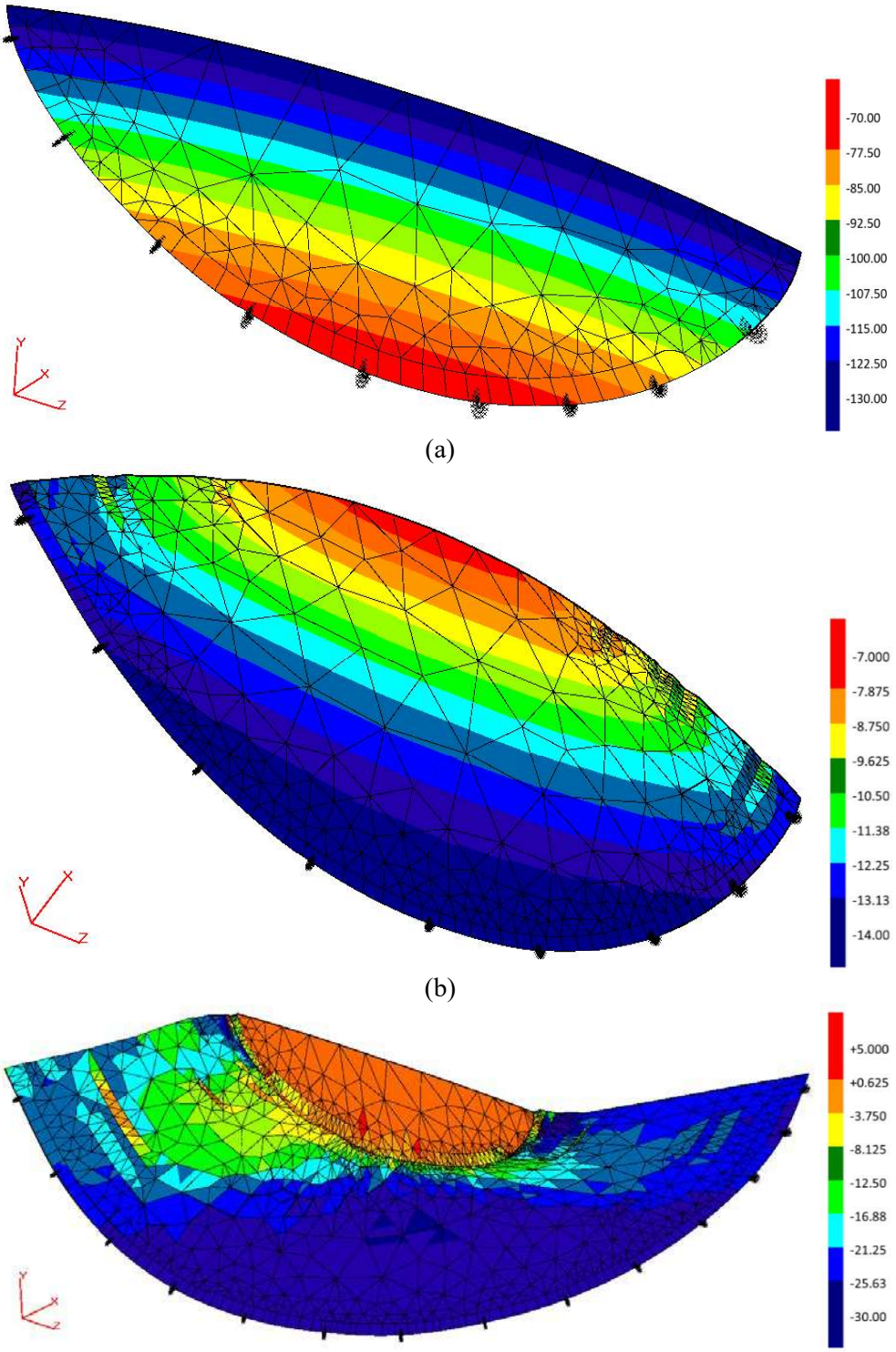

Fig. 13. Contour plots of normal tractions (MPa) as applied to final crack: “coupled” (a), “shear” (b), “torque” (c).